ISBN: 978-3-95450-232-5 ISSN: 2673-7000 doi:10.18429/JACoW-NAPAC2022-MOPA85

DESIGN OF A 185.7 MHz SUPERCONDUCTING RF PHOTO-INJECTOR QUARTER-WAVE RESONATOR FOR THE LCLS-II-HE LOW EMITTANCE INJECTOR*

S. Kim[†,1], C. Adolphsen[4], L. Ge[4], W. Hartung[1], F. Ji[4], M. Kelly[2], T. Konomi[1], J.W. Lewellen[4], S. Miller[1], M. Patil[1], T. Petersen[2], P. Piot[2,3], J. Popielarski[1], K. Saito[1], L. Xiao[4],T. Xu[1], T. Xu[1],
[1]Facility for Rare Isotope Beams, Michigan State University, East Lansing, MI, USA
[2]Argonne National Laboratory, Argonne, IL, USA
[3]Northern Illinois University, DeKalb, IL, USA
[4]SLAC National Accelerator Laboratory, Menlo Park, CA, USA

Abstract

A 185.7 MHz superconducting quarter-wave resonator (QWR) was designed for the Low Emittance Injector of the Linac Coherent Light Source high energy upgrade (LCLS-II HE LEI). The cavity was designed to minimize the risk of cathode efficiency degradation due to multipacting or field emission and operate with a high RF electric field at the cathode for low electron-beam emittance. Cavity design features include (1) shaping of the cavity wall to reduce the strength of the low-field coaxial multipacting barrier; (2) four ports for electropolishing and high-pressure water rinsing; (3) a fundamental power coupler (FPC) port located away from the accelerating gap. The design is oriented toward minimizing the risk of particulate contamination and avoiding harmful dipole components in the RF field. The ANL 162 MHz FPC design for PIP-II is being adapted for the gun cavity. We will present the RF design of the cavity integrated with the FPC.

INTRODUCTION

SLAC plans to upgrade its LCLS-II to produce higher-energy X-rays for X-ray Free Electron Laser (XFEL) users. It is planned to add more accelerating cryomodules in linac to increase the electron beam energy and also to upgrade the injector to generate ultra-low emittance (~0.1 μm·rad at 100 pC bunch chage) electron beam: LCLS-II High Energy upgrade (HE) Low-Emittance Injector (LEI) [1, 2]. The approach for the electron gun is use of a superconducting radiofrequency (SRF) gun in order to provide stable CW operation and a low-frequency option such as 185.7 MHz was chosen to minimize growth of the projected emittance due to time-dependent transverse RF field [3].

Michigan State University (MSU) – Argonne National Laboratory (ANL) – Helmholtz Zentrum Dresden Rossendorf (HZDR) collaboration team was selected to develop an SRF gun cryomodule integrating with a cathode load-lock system. We chose these technical options for the SRF cavity and FPC [1]: 185.7 MHz quarter-wave resonator (QWR), two-window fundamental power coupler (FPC) based on ANL's 162 MHz FPC as used in the PIP-II HWR cryomodule [4].

* Work supported by the Department of Energy Contract DE-AC02-76SF00515.
[†]kims@frib.msu.edu

One of the design goals is the RF electric field at the cathode E_c (cathode gradient) higher than 30 MV/m, which has never been demonstrated in the other 'production' SRF guns that provided beams for user operations [5, 6]. The challenges of the past SRF guns in achieving such high cathode gradient were conditioning effects or excessive dark currents due to field emission and/or multipacting [5]. We designed our cavity integrated with an FPC improved from the past low-frequency SRF guns. In particular, these features are employed, as shown in Fig. 1:

- The anode-side cavity end wall is a "dome" shape, which helps to reduce the strength of low-field coaxial multipacting barrier,
- The cavity is equipped with four rinse ports that allows electropolishing and high-pressure rinsing,
- The FPC is installed on a rinse port instead of the beam port while not introducing harmful dipole mode. This was chosen to reduce possible field emission due to potential particulate cross-contamination during clean assembly.

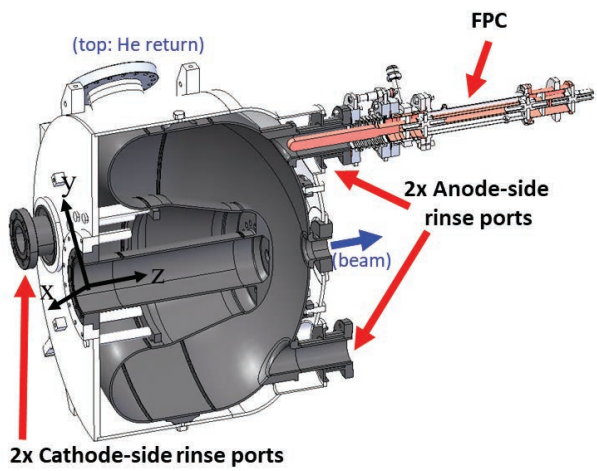

Figure 1: He-jacketed SRF Gun cavity integrated with the fundamental power coupler (FPC). This is a cross-sectional view on a 'skew' plan; x: horizontal, y: vertical, z: longitudinal axes. Another cathode-side rinse port exists on the other side of this view.

These are based on the experience with development and operation of low-frequency, low-β SRF cavities and cryomodules [7, 8]. We will present the details of cavity

ISBN: 978-3-95450-232-5 ISSN: 2673-7000 doi:10.18429/JACoW-NAPAC2022-MOPA85

design and impacts of FPC integration in this paper. The other SRF subsystems will be discussed elsewhere [1, 9].

CAVITY DESIGN

Preliminary beam dynamics study suggested the accelerating gap distance of 70 mm and the beam pipe diameter of 40 mm. The inner-conductor end region around cathode, indicated by "A" in Fig. 2, is based on the WiFEL gun geometries that was designed to minimize the transverse field at cathode and also to reduce E-field enhancement at the corner of the inner-conductor end [10]. The anode region, indicated by "B" in Fig. 2, has a large-radii elliptical blend, chosen to reduce the strength of potential low-field multipacting barriers. With this large elliptical blend, the multipacting strength is expected to be lower than the previous WiFEL gun cavity as shown in Figs. 3 and 4. In case of the WiFEL gun, the low-field multipacting barrier needs more than 20 hours CW conditioning, which will not be favorable for reliable user operation [11]. Regarding the short-plane, we investigated effect of the short-plane radius *R* on SRF cavity parameters such as *r/Q* (calculated assuming a speed-of-light particle), *G*, E_{peak}, B_{peak} as well as the multipacting strength and found that a larger R is favorable; *r/Q* and *G* are improved, Increase of E_{peak}, is marginal, B_{peak} is increased but it is still at a 'moderate' level, ~50 mT. We finally chose R of 75 mm, balancing concerns about the mechanical stiffness of the inner conductor against df/dp and Lorentz force detuning effect.

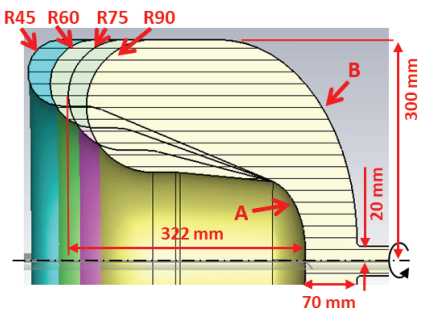

Figure 2: 2-D model cavity shapes in various options of the short-plane radius R.

Beam and rinse ports were added into the 3-D cavity model; E and B-field are as shown in Fig. 5. B-field is enhanced at the transitions of the short-plane rinse ports as shown in Fig. 5 (b), however, the maximum B-field is 53 mT, believed to be still a moderate level so that no further efforts to enlarge the blend radius of the transition is necessary. The corners of the cathode and niobium-cavity cathode-hole have an elliptical profile, as shown in Fig. 6, such that E-field at the corners does not significantly exceed E_{peak} as in the model without the cathode hole.

The cavity helium jacket, as also shown in Fig. 1, was designed to minimize the frequency sensitivity to the helium bath pressure df/dp as well as to withstand at the maximum allowable pressure of the helium vessel.

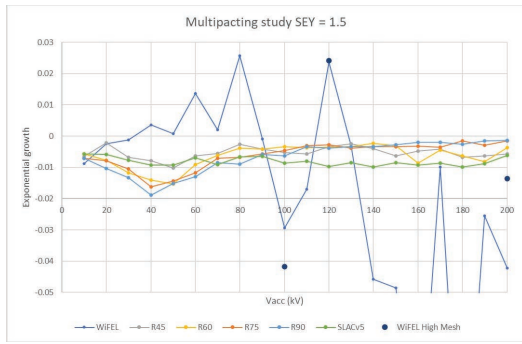

Figure 3: Growth rates of multipacting electrons in the models with various R from 45 mm to 90 mm, compared to the WiFEL gun.

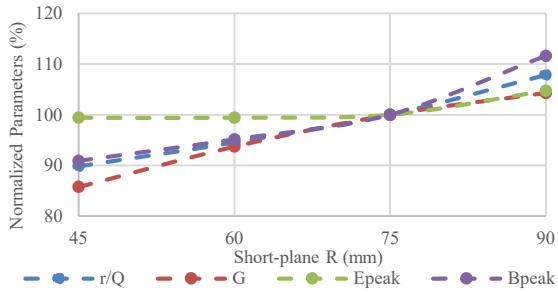

Figure 4: Cavity parameters such as *r/Q*, geometric factor *G*, peak surface electrical and magnetic field E_{peak}, B_{peak}, normalized to those in the R75 model. Absolute values in the R75 model are: *r/Q* = 131 Ohm, *G* = 84.5 Ohm, E_{peak} = 34 MV/m, B_{peak} = 47 mT, the last two of which are when Ec = 30 MV/m.

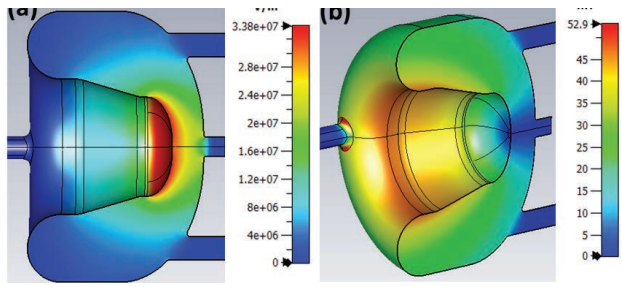

Figure 5: Left: E-field. Right: B-field in the nominal condition, E_c = 30 MV/m. This model does not include the cathode hole.

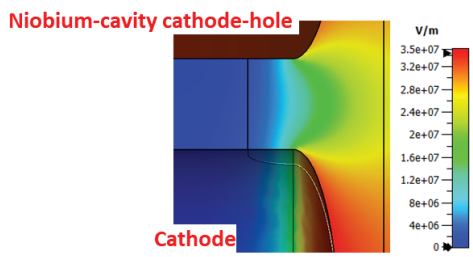

Figure 6: E-field strength around the cathode and the cathode-hole of the niobium cavity.

The df/dp together with the other parameters of the jacketed cavity are as shown in Table 1. Note that the Lorentz force detuning is normalized to the stored energy of 1 J instead of representing in the unit of Hz/(MV/m)^2

ISBN: 978-3-95450-232-5 ISSN: 2673-7000 doi:10.18429/JACoW-NAPAC2022-MOPA85

because the conventional definition of the effective length $L_{eff} = \beta\lambda/2$ is not relevant to this highly re-entrant single-gap cavity. Frequency shifts due to this LFD effect is expected to be similar to the case of FRIB half-wave resonators and, thus, the static LFD effect is not of concern [7].

Table 1: Cavity Design Parameters

Parameter	Value
Operating Temperature	4.2 K
Frequency	185.7 MHz
Accelerating gap distance	70 mm
Short-plane radius R	75 mm
r/Q	131 Ohm
Geometric factor $G = Q_0 * R_s$	84.5 Ohm
Cathode gradient E_c	30 MV/m
Integrated E_z field*	1.8 MV
Peak surface electric field E_{peak}*	34 MV/m
Peak surface magnetic field B_{peak}*	53 mT
Frequency sensitivity to helium-bath pressure $\lvert df/dp \rvert$	< 4 Hz/Torr
Lorentz force detuning	-29 Hz/J
Frequency tuning sensitivity df/dx	-435 kHz/mm
Coarse frequency tuning range	60 kHz
Required tuning force	8.4 kN

*At the nominal condition, E_c = 30 MV/m

FPC INTEGRATION

The FPC assembly integrated with the cavity and cryomodule is designed such that the coupling strength can be adjusted from outside of the cryomodule [4]. The designed lowest Qext in the adjustable range is 6×10^5 as shown in Fig. 7 in order to support high-peak power pulsed RF conditioning and room-temperature plasma processing, while the nominal Qext is 1×10^7 for operation. The highest Qext for plasma processing is limited to avoid plasma generation in the FPC space instead of the cavity space.

The B-field on the anode plane is not negligible, as shown in Fig. 5 (b), somewhat different from typical QWRs for low-β accelerators. This is likely due to a relatively large cavity outer-conductor diameter compared to the cavity length. Antenna heating due to H-field at the antenna tip was investigated; coupled RF-thermal analysis together with fluid simulation on cooling of the FPC cold window by 55 K gas helium concluded that the dissipation power and temperature rise are acceptable, as shown in Fig. 8.

The FPC cold window will not be directly hit by field emission (FE) electrons. Figure 9 shows FE electron trajectories at one RF phase; at the other RF phases, FE electron stopping locations with respect to the cold window position are not so different from this case.

The coupler multipacting is expected to be fully suppressed by DC bias voltage higher than 200 V, as already demonstrated in ANL's 162 MHz FPC [4].

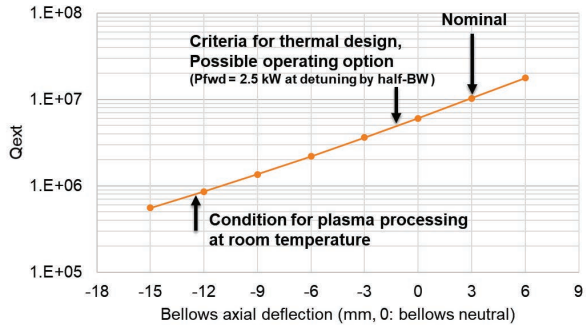

Figure 7: The variable range of the coupling strength that can be provided by the FPC design.

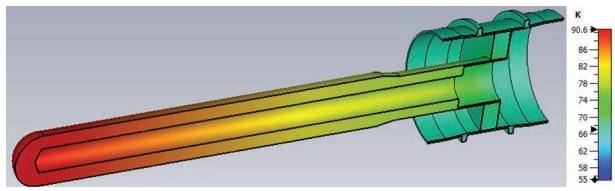

Figure 8: FPC antenna heating due to RF H-field. A major source of heating is the cavity H-field around the antenna tip and wall dissipation power is 13 W.

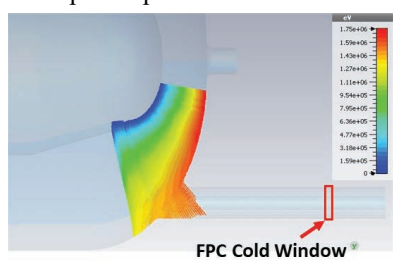

Figure 9: Trajectories of field-emission electrons assuming emitted from the inner conductor. This is when E_c is at the nominal condition and the RF phase is at the crest.

SUMMARY

The SRF gun cavity and FPC were designed for LCLS-II HE LEI. We improved the cavity and FPC design from the past low-frequency SRF guns to mitigate potential impacts due to possible multipacting and field emission. This design incorporate the experience in designing, building, testing, and operating low-β, low-frequency cavities and FPCs at FRIB and ANL.

Regarding validation of cavity and FPC design, we plan the jacketed-cavity cold test at FRIB, cavity integration test with FPC and tuner at ANL, both in 2023.

ACKNOWLEDGEMENTS

The authors greatly thank to the HZDR collaboration team and R. Legg at SLAC for sharing their experience in SRF gun test and operation.

REFERENCES

[1] J. W. Lewellen *et al.*, "Status of the SLAC/MSU SRF Gun Development Project", presented at the NAPAC'22, Albuquerque, New Mexico, USA, Aug. 2022, paper WEPA03, this conference.

ISBN: 978-3-95450-232-5 ISSN: 2673-7000 doi:10.18429/JACoW-NAPAC2022-MOPA85

[2] F. Ji *et al.*, "Beam dynamics studies of a low emittance injector for LCLS-II HE", presented at the NAPAC'22, Albuquerque, New Mexico, USA, Aug. 2022, paper WEPA02, this conference.

[3] K.J. Kim, "Rf and space-charge effects in laser-driven rf electron guns", *Nucl. Instrum. Methods Phys. Res. A,* vol. 275, pp. 201-218, 1989.

[4] M.P. Kelly *et al.,* "Coaxial Power Coupler Development at Argonne National Laboratory", in *Proc. SRF'17*, Lanzhou, China, Jul. 2017, paper FRXBA03, unpublished.

[5] "Future of Electron Sources", Report of the BES Workshop on the Future of Electron Sources, Sep. 2016, Menlo Park, CA, USA.

[6] R. Xiang, "Review of Superconducting Radio Frequency Gun", in *Proc. IPAC'21*, Campinas, Brazil, May 2021, pp. 2556-2561. doi:10.18429/JACoW-IPAC2021-WEXC03

[7] T. Xu *et al.,* "Completion of FRIB Superconducting Linac and Phased Beam Commissioning", in *Proc. SRF'21*, East Lansing, MI, USA, Jun.-Jul. 2021. doi:10.18429/JACoW-SRF2021-MOOFAV10

[8] Z. A. Conway, B. M. Guilfoyle, M. Kedzie, M. P. Kelly, T. Reid, and H. Guo, "Progress Toward 2 K High Performance Half-wave Resonators and Cryomodule", in *Proc. SRF'17*, Lanzhou, China, Jul. 2017, pp. 692-694. doi:10.18429/JACoW-SRF2017-WEYA05

[9] T. Konomi *et al.*, "Design of the Cathode Stalk for the LCLS-II-HE Low Emittance Injector", presented at the NAPAC'22, Albuquerque, New Mexico, USA, Aug. 2022, paper MOPA87, this conference.

[10] R. Legg *et al.*, "Wisconsin SRF Gun Development", in *Proc. ERL'09*, Ithaca, NY, USA, Jun. 2009, paper WG118, pp. 45-49.

[11] T. B. Petersen *et al.,* "Refurbishment and Testing of the WiFEL E-Gun at Argonne", in *Proc. SRF'21*, East Lansing, MI, USA, Jun.-Jul. 2021. doi:10.18429/JACoW-SRF2021-WEPCAV015